# Hydro-plastic response of beams and stiffened panels subjected to extreme water slamming at small impact angles, Part II: Numerical verification and analysis

Zhaolong Yu [a, b*], Jørgen Amdahl [a, b], Marilena Greco [a, b, c], Huili Xu [a, b]

a, Centre for Autonomous Marine Operations and Systems (AMOS), Norwegian University of Science and Technology (NTNU), Norway

b, Department of Marine Technology, Norwegian University of Science and Technology (NTNU), Norway

c. CNR-INM, Institute of Marine Engineering, Rome, Italy

## Abstract

An analytical model has been proposed for the response of beams and stiffened panels subjected to extreme flat or nearly flat water impacts in Part I of the two-part companion paper. The model aims to capture the significant hydro-plastic coupling between large plastic structural deformations and the hydrodynamic pressure. Governing non-dimensional parameters for the hydro-plastic slamming phenomenon were identified and discussed.

This Part II paper verifies the analytical model proposed in Part I by comparison with the hydro-plastic slamming response of beams and stiffened panels using multi-material Arbitrary Lagrangian Eulerian (ALE) methods in LS-DYNA. Numerical modeling and settings with the ALE simulations are firstly validated by comparison against drop-test experiments of a *rigid* wedge and of an *elastic* plate. Then, water entry simulations of flat plates and stiffened panels are carried out, where structural deformations go into the *plastic* regime. The simulated scenarios cover different plate thicknesses/cross sectional dimensions of stiffened panels, and various initial water-entry velocities. The analytical model is discussed with respect to the fluid flow, structural deflections, the pressure history and the impulse. Validity of assumptions of the analytical model is also discussed. Potential applications and limitations are indicated. The proposed design curves are well suited to be utilized in rules and standards for designing against extreme water slamming.

**Key words**: water slamming; hydro-plasticity; beams and stiffened panels; ALE simulations; verification; design curves

## 1. Introduction

Water impacts are known to occur for ships and offshore structures at sea due to relative motions between the liquid and the structure. Example scenarios leading to slamming are water entry and exit of ship bow and stern, offshore platforms subjected to steep breaking waves, high speed vessels travelling in waves and free-falling life boats. Structures subjected to impulsive loads from water slamming, may respond in the elastic or elastoplastic regimes depending on the load intensity, and there can be significant coupling effect between water pressure and the structural response, termed as hydroelasticity and hydro-elastoplasticity, respectively. Hydroelastic slamming has been studied extensively, for instance by Faltinsen (2000), Kvalsvold and Faltinsen (1995), Bishop and Price (1979) and Qin and Batra (2009), but similar attention has not been given to the hydro-elastoplastic or hydro-plastic slamming. In practice, offshore structures may be impacted by steep and energetic waves in extreme sea states, causing significant structural damage. For example, the accident of the offshore drilling rig *COSL Innovator* in the North Sea in 2015 led to one death and extensive damage to the cabins after being struck by an energetic horizontal wave. In order to maintain structural safety and to prevent such accidents to occur, rules and standards should be established for designing against extreme slamming loads.

For structural design in the Ultimate Limit State (ULS) conditions subjected to slamming, simple guidelines were introduced in DNVGL-OTG-13 (2016) for the air gap calculation and in DNVGL-OTG-14 (2016) for providing the temporal and spatial distributions of the design slamming loads. The rules focus on the peak pressure, the shape of the pressure impulse, the impulse duration and the pressure spatial distribution. Similarly, a few researchers studied plastic response of structures subjected to extreme slamming by assuming a certain temporal and spatial pressure distribution, such as Jones (2011), Jiang and Olson (1995) and Henke (1994). These methods, however, neglect the hydro-elastoplastic coupling between the structural response and water pressure, and do not reflect the real physics behind the phenomenon.

Literature review has shown that limited knowledge exists for scenarios where the plastic response of a structure becomes dominant in the Accidental Limit States (ALS) conditions. In order to bridge the knowledge gap and to obtain a deeper understanding of the hydro-plastic slamming phenomenon, Part I (Yu et al., 2019) of the two-part companion paper firstly formulated an analytical solution for the hydro-plastic response of beams and stiffened panels subjected to extreme water slamming. Based on the analytical model, governing non-dimensional parameters were identified and discussed. The objective of this Part II paper is to assess the analytical model and to discuss its potential applications and limitations. The assessment requires comparisons against reliable reference solutions using experiments or numerical simulations.

Quite a few experiments on slamming impacts are reported in the literature. However, they were mainly designed to study the slamming pressure on rigid bodies or the hydroelastic coupling between fluid and the structure. Very few experiments were carried out with extreme slamming loads that were capable of producing large inelastic structural damage. Shin et al. (2017) carried out repeated drop tests of unstiffened plates into a rectangular tank and recorded the cumulative plate damage. However, because of the small tank size, one can expect that the hydrodynamic pressures can be significantly affected by the confined water. In addition, because of the limited

drop height, the deformations after the first drop were generally in the elastic range. On the numerical side, a few numerical simulations with the Arbitrary Lagrangian Eulerian (ALE) method were carried out to study the elastoplastic responses of the structures to slamming, such as Cheon et al. (2016), Luo et al. (2010), Yamada et al. (2012) and Skjeggedal (2017). In the ALE method, the structures are modelled with Lagrangian meshes while the fluid domain including water and air is discretized with Eulerian meshes. Upon iterations, the hydrodynamic pressure and boundary conditions are transferred between the structural and fluid domains.

Based on this, this Part II paper verifies the proposed analytical model in the Part I paper by means of multi-material ALE simulations using LS-DYNA. Numerical settings of the ALE simulations are validated with the *rigid*-wedge drop tests by Zhao et al. (1996) and drop tests of *elastic* flat plates by Faltinsen et al. (1997). Water entry simulations are then carried out for the flat plate strips and stiffened panels with different cross sectional dimensions and impact velocities. The analytical model is discussed with respect to the fluid flow, structural deflections, the pressure history, and the impulse. Potential application and limitations of the analytical method are discussed.

## 2. A summary of the analytical model and findings from Part I

### *2.1 The analytical model for hydro-plastic slamming*

The analytical model proposed in Part I (Yu et al., 2019) assumes that in the extreme slamming events in ALS conditions, the elastic energy of a structure is small compared to the plastic energy such that all the kinetic energy should be dissipated by plastic deformations. The perfectly plastic material is often adopted in other ALS conditions with good accuracy, such as collisions and groundings (Yu and Amdahl, 2018). During hydro-plastic slamming of flat beams, the response is categorized into two phases, i.e. the structural inertia phase (also called the acoustic phase) and the free deflection phase. In the structural inertia phase, the structure is subjected to an intensive pressure impulse with a large pressure peak and a short duration. At the end of the structural inertia phase, the structure is assumed to be imparted a deformation velocity equal to the initial drop velocity $V_0$ in the beam middle portion between the two travelling hinges. The deformation velocity decreases linearly to zero from the travelling hinges to the beam ends. The duration of the structural-inertia phase is, however, too short for the structure to build up any deflection. These are considered as initial conditions of the free deflection phase.

In the free deflection phase, the structure deforms and may undergo three deformation stages, i.e. the travelling hinge stage 1, the stationary hinge stage 2 and the pure tension stage 3 (refer Fig. 1). In stage 1, travelling hinges form at a certain distance $X$ from the beam ends and move towards the middle. The beam portion between the hinges has a constant velocity $V_m$ equal to the initial impact velocity $V_0$ (refer Fig. 1(a)). When the travelling hinges merge in the middle, the stationary hinge stage 2 starts and the beam middle velocity starts to decrease over time. During the deflection, the beam bending moment and axial membrane force interact through the generalized interaction curves. For stiffened panels, the interaction functions are taken from Yu et al. (2018). For beams fixed at the ends, when the beam middle deflection $\delta$ reaches the beam height $h$, the beam cross section becomes fully occupied by membrane forces, and the pure tensile stage 3 starts. The permanent deflection is reached when the beam middle velocity $V_m$ decreases to zero.

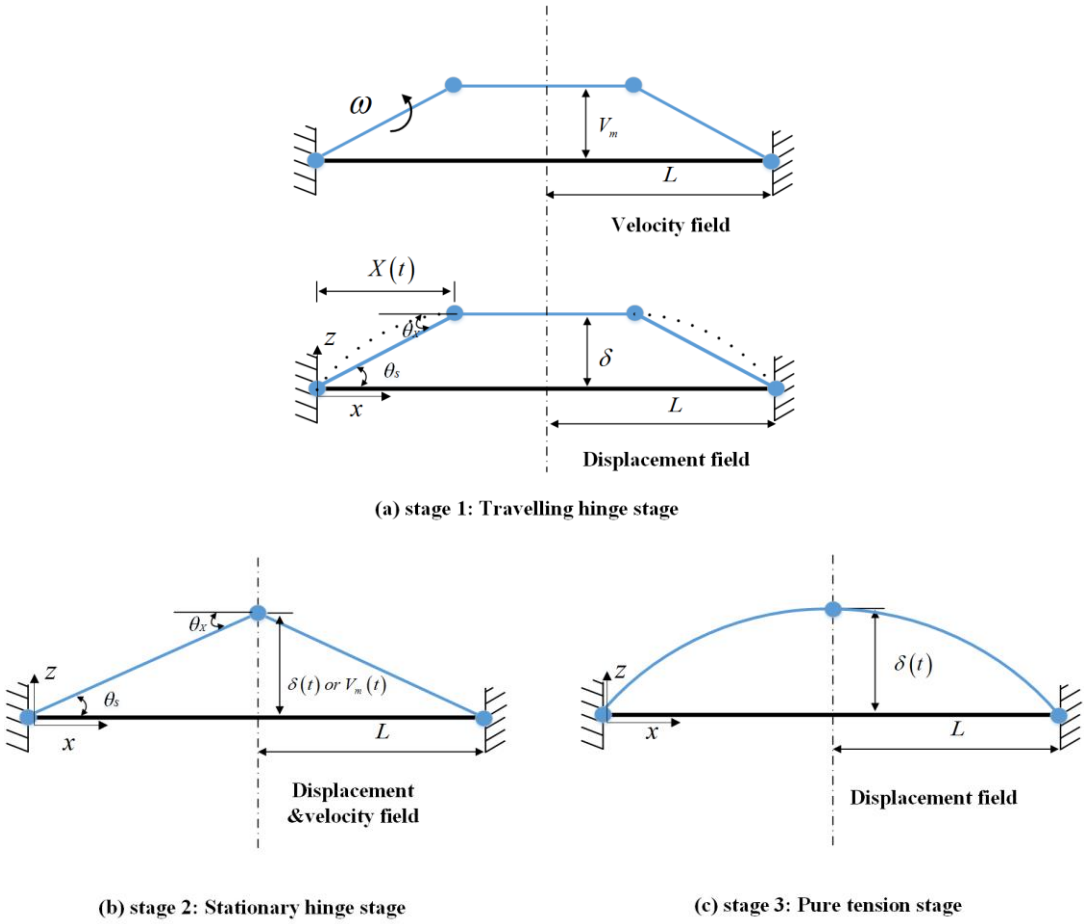


Fig. 1. Deformation stages of a beam during the free-deflection phase induced by slamming

During the deformations, significant coupling exists between the beam plastic deflection and the water pressure, denoted as hydro-plasticity. In stages 2 and 3, water pressure acts as an added mass effect and pushes the decelerating structure to deform. For stage 1, apart from an added-mass term, we have a second pressure term related to an added-mass time change effect due to the moving hinges leading to a change in the structural mode.

By equating the rate of internal and external work, the governing motion equations are found, and are solved numerically with the fourth order Runge-Kutta method.

### *2.2 Governing non-dimensional parameters*

For the hydro-plastic slamming response of flat plate strips, i.e. two-dimensional (2D) flat plates, three governing non-dimensional parameters have been identified, which are,

- The non-dimensional velocity $V_{nd} = V_0 \sqrt{\dfrac{\rho L^3}{M_0 h / b}}$
- The mass ratio $m_{nd} = m / \rho b L$

- The ratio of initial travelling hinge position over half of the beam length $X_{nd} = \dfrac{X(t=0)}{L} = \sqrt{\dfrac{24}{\left(V_0\sqrt{\dfrac{\rho L^3}{M_0 h/b}}\right)^2}\cdot\dfrac{V_0 L}{c_e h}}$

For the hydro-plastic response of stiffened panels, two more parameters are identified in addition to the three above:

- The area ratios $A_{ps,nd} = A_p / A_s$ and $A_{wt,nd} = A_w / A_t$

Here, $V_0$ is the initial impact velocity, $\rho$ is the water density and $L, b, h$ are, respectively, the length, width and height of the beam. $m$ is the mass of a beam per unit length, $X(t=0)$ is the initial position of a travelling hinge from the corresponding beam edge. $c_e$ is the speed of sound in water. $M_0$ is the fully plastic bending moment for the beam cross section. $M_0 = 1/4\sigma_y bh^2$ for rectangular beams and $M_0 = \sigma_y (A_t + A_w/2)h$ for stiffened panel cross sections. $A_p$, $A_w$, $A_t$ are the area of the plate flange, area of the web and area of the top flange, respectively. $A_s = A_t + A_w$ is the area of the stiffener. A complete definition of the symbols is provided in Part I (Yu et al., 2019).

It is found that the non-dimensional velocity $V_{nd}$ is the most crucial parameter that dominates the hydro-plastic response of beams and stiffened panels. Stiffened panels with large web heights, *h*, are mainly governed by stages 1 and 2 deformations. The permanent deflection $\delta_p / h$ increases nonlinearly with the non-dimensional velocity. For plates, the characteristic dimension *h* is much smaller than the stiffener spacing, and the response is mainly governed by stage 3. $\delta_p / h$ increases virtually linearly with the non-dimensional velocity.

The area ratios $A_p / A_s$ and $A_w / A_t$ are important parameters for stiffened panels. Permanent deflections increase with decreasing $A_p / A_s$ and $A_w / A_t$ ratios for a given non-dimensional velocity, and the $A_p / A_s$ ratio is dominant. The influence of the mass ratio $m / \rho bL$ is limited.

## 3. Validation of ALE simulation with experiments

The explicit NLFEM code LS-DYNA version 971 (Hallquist, 2007) with the multi-material ALE algorithm was employed to verify the analytical formulas. Prior to the simulation of *hydro-plastic* slamming, validation of the numerical setup and the accuracy of simulation results were assessed by comparison with a 2D *rigid*-wedge drop test by Zhao et al. (1996) and the drop test of a horizontal flat *elastic* plate by Faltinsen et al. (1997).

### *3.1 Numerical set-up of ALE simulations*

Water and air are modelled with multi-material Eulerian meshes while the structure is modelled with Lagrangian meshes. Coupling is enabled in a way that the Lagrangian structure domain imposes displacement and velocity boundary conditions on the Eulerian fluid, which in return

imposes hydrodynamic pressure on the structure. The water and air domains are modelled using the 1 point ALE multi-material solid elements. Material properties of the fluids are defined with the NULL materials and the linear polynomial equation of state (EOS). The properties adopted for water and air are listed in Table 1. The values have been validated by Bae and Zakki (2011) through comparison with experiments.

Table 1 EOS linear polynomial parameters for water and air, from Bae and Zakki (2011)

| | Water | Air |
|---|---|---|
| Density (kg/m$^3$) | 1025 | 1.225 |
| $C_0$ | 0 | 0 |
| $C_1$ | $2.002 \cdot 10^9$ | 0 |
| $C_2$ | $8.436 \cdot 10^9$ | 0 |
| $C_3$ | $8.010 \cdot 10^9$ | 0 |
| $C_4$ | 0.4394 | 0.4 |
| $C_5$ | 1.3927 | 0.4 |
| $C_6$ | 0 | 0 |
| $E_0$ | $2.086 \cdot 10^5$ | $2.5 \cdot 10^5$ |
| $V_0$ | 1 | 1 |

The penalty-based coupling method is applied to model contact between the fluid and the structure. During contact, the fluid nodes are allowed to have a small penetration into the structure. Resisting forces are then imposed between the contact points on the structural elements and the fluid nodes. The penalty factor corresponding to the contact stiffness of interacting bodies is set to the default value of 0.1. The contact damping is selected to be 0.9 times the critical damping according to Stenius et al. (2006). The fluid-structure coupling takes place in the normal direction to the body surface when the fluid tends to enter the structure, i.e. in compression only.

### *3.2 Validation of the numerical code with drop tests*

#### *3.2.1 2D rigid-wedge drop test*

Zhao et al. (1996) carried out a drop test of a 2D rigid wedge in MARINTEK. The deadrise angle of the rigid wedge was 30$^o$ and the drop height was 2 m. The main dimensions of the tested section are shown in Table 2.

A 2D model is established in LS-DYNA as shown in Fig. 2. Because the problem is symmetric with respect to the body central axis, only half of the domain is modelled. The water domain is 0.75 m in width and 0.5 m in depth while the dimension of air domain is 0.75 m$\times$0.4 m. Both the fluid and structure domains are discretized with a uniform mesh size of 2.5 mm. In the thickness direction, one element was modelled for the fluid domains. Nodal velocities in the fluid domains are fixed in the *y* direction to enable a 2D fluid flow. The nodes along the left wall of the fluid domain are constrained in the *x* direction to enforce the symmetry condition. Elements of mass points are added to the top of the rigid wedge such that the mass of the experimental wedge including ballast weights, is reproduced exactly. The time step size is automatically calculated by the LS-DYNA solver. The value is very small and is typically in the order of $10^{-6}$ s.

Table 2. The main data of the test sections (Zhao et al., 1996)

| | |
|---|---|
| Breadth of section | 0.50 m |
| Length of measuring sections | 0.20 m |
| Length of each dummy sections | 0.40 m |
| Total length | 1.00 m |
| Weight of drop rig (without ballasts) | 141 kg |
| Ballast weight | 100 kg |
| Total weight of the drop rig | 241 kg |
| Weight of the measuring section | 14.5 kg |

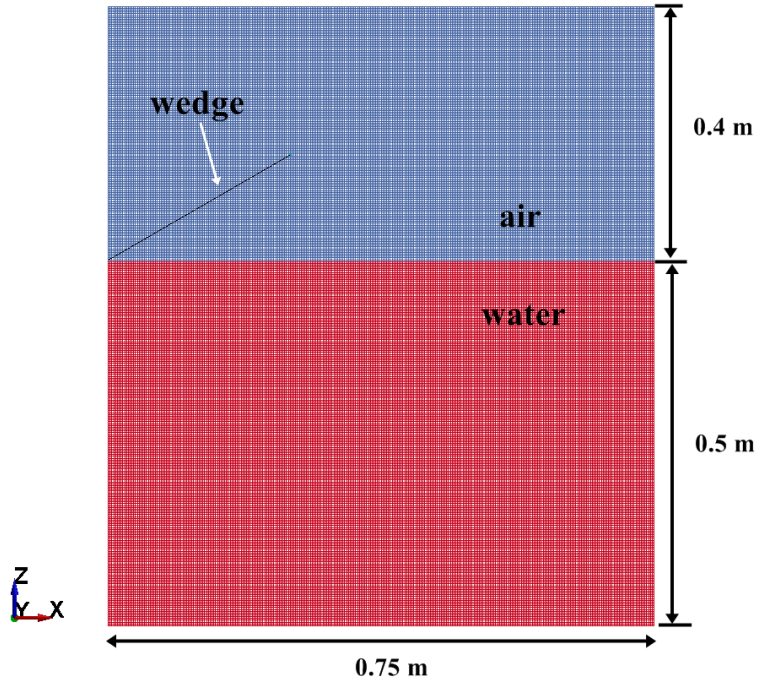


Fig. 2. Initial instant of the drop test simulation of the rigid wedge in LS-DYNA, and the initial velocity is equal to the measured velocity from the experiment before impacting the water.

A snapshot of the flow field of water and air simulated during water entry is given in Fig. 3. At this stage, the water rise-up along the wedge produced a jet detached from the structure. The water jet, water-air mixture and flow separation are reasonably captured. The local details of the jet cannot be considered accurate when the related dimensions are comparable to the local cell size. This has consequences on the further jet evolution and on the local mass conservation, but the effects for the fluid-body interaction during the slamming are expected to be limited. This is confirmed by Fig. 4 that compares water-entry forces acting on the wedge from the ALE simulation and from the experiment. Except for the initial oscillations, the simulation agrees well with the measurement both in terms of behaviors and maximum values.

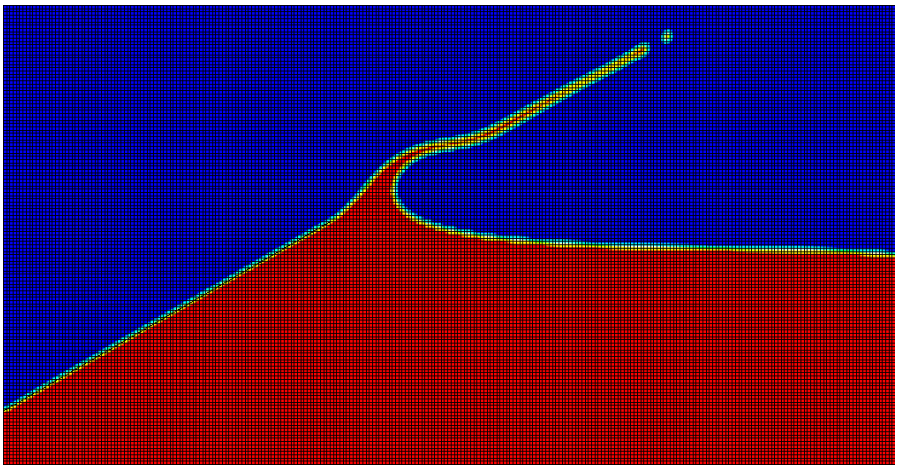

Fig. 3. Water jet during water entry of a rigid wedge. The red region identifies the water; the blue region, the air; the green region, the numerical smoothed transition from water to air.

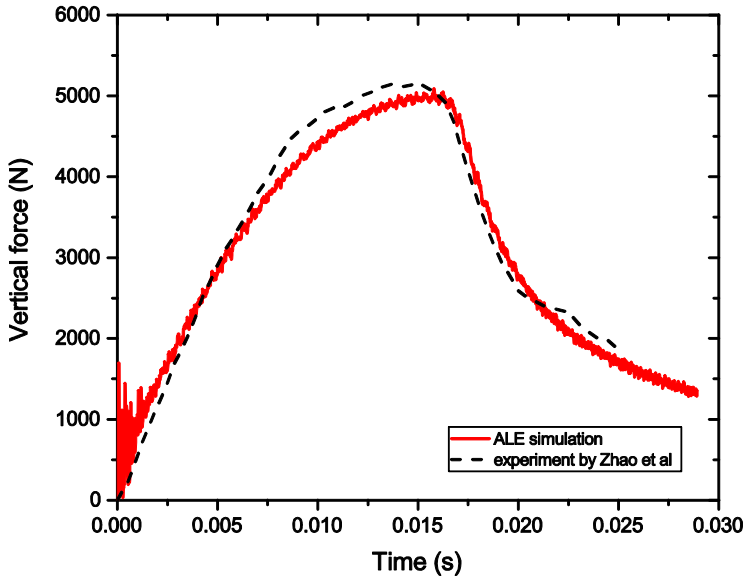


Fig. 4. Comparison of water-entry forces from ALE simulation and experiments by Zhao et al. (1996)

### *3.2.2 Elastic flat plate drop test*

Faltinsen et al. (1997) conducted a drop test with a horizontal flat elastic plate. The main parameters for the plate are shown in Table 3. The drop height is 0.5 m, yielding a measured velocity of about 3.03 m/s when water entry starts.

The 2D model is established in LS-DYNA as shown in Fig. 5. Half of the domain is modelled due to symmetry conditions. The water domain is 0.5 m in width and 0.5 m in depth while the dimension of air domain is 0.5 m$\times$0.2 m. The water and air domains, as well as the plate, are discretized with a mesh size of 2.5 mm. Nodal velocities in the fluid domains are fixed in the *z* direction to enable

a 2D fluid flow. The nodes along the right wall of the fluid domain are constrained in the *x* direction to enforce the symmetry.

In order to model the rotational stiffness at the plate boundary consistently with the model tests, an elastic beam connects the support to a rigid plate as shown in Fig. 5. The length and the elastic modulus of the beam are calibrated to reproduce the rotational stiffness in the experiment. Mass points are distributed along the boundaries to reproduce the same mass of the experimental plate, including ballast weights.

Table 3. The main data of the plate used in the drop test by Faltinsen et al. (1997)

| | |
|---|---|
| Structural mass per unit length and breadth | 62 kg/m$^2$ |
| Modulus of elasticity | $2.1 \cdot 10^{11}$N/m$^2$ |
| Length of plate | 0.5 m |
| Breadth of plate | 0.1 m |
| Bending stiffness | 8960 Nm$^2$/m |
| Connecting spring parameter | 102144 Nm/(rad$\times$m) |
| Plate thickness | 8 mm |
| Total weight | 500 kg |

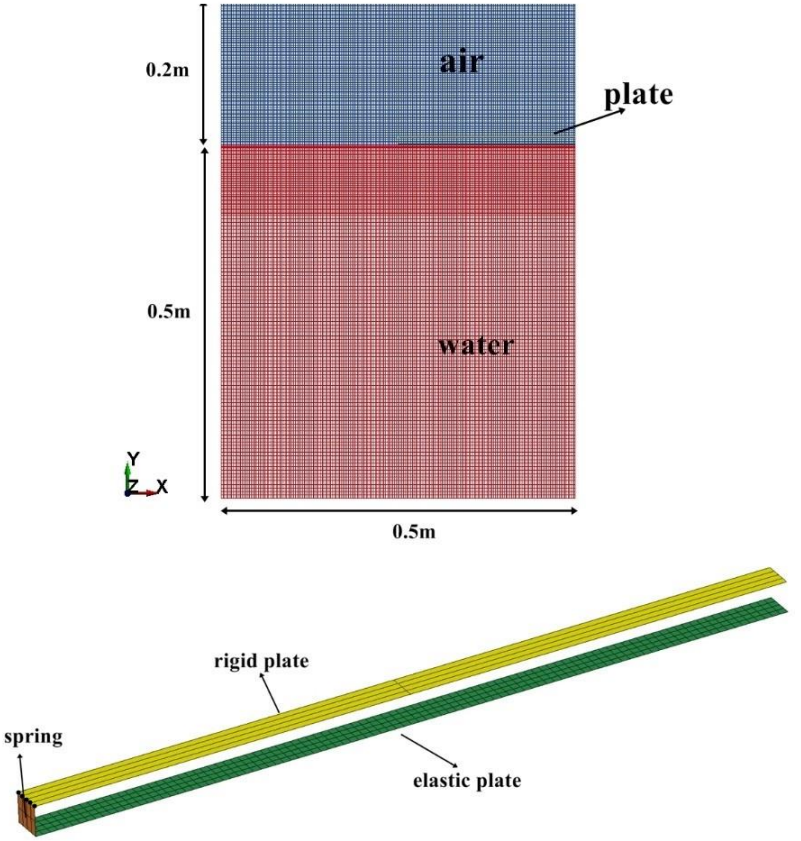


Fig. 5. Top: Initial instant of the water entry simulation of a flat elastic plate in LS-DYNA, and the initial velocity is equal to the measured velocity from the experiment before impacting the water. Bottom: numerical plate

Fig. 6 compares the pressures obtained in the simulation and measured in the experiment. The peak pressure and the pressure during plate vibration are in good agreement with the experimental ones.

Negative pressure is not captured in the ALE simulation because the initial atmospheric pressure is not modelled. This is consistent with the observation of Wang et al. (2016), who also simulated this experiment with the ALE formulation. According to the experiment, the negative pressure, i.e. relative to the atmospheric pressure, leads to the cavitation and ventilation phenomena, and is not captured numerically. This effect is considered secondary for the maximum deflections and stresses induced by slamming on the plate.

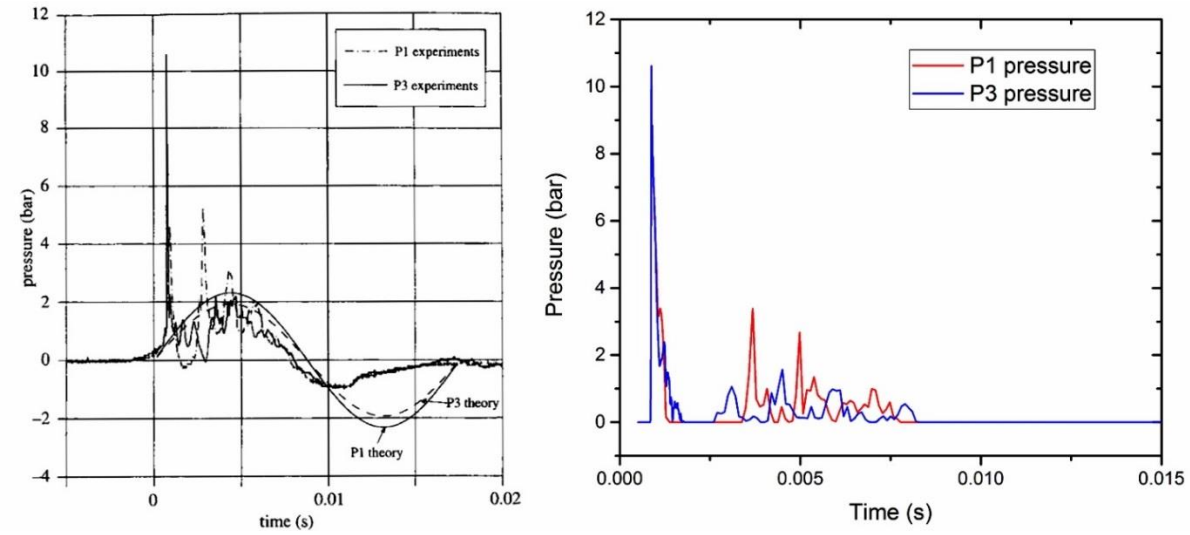


Fig. 6. Comparison of pressure during water entry of a flat elastic plate. Left: measured pressure from experiment by Faltinsen et al. (1997); Right: pressure from ALE simulations with a moving average. P1 is pressure at the plate midpoint and P3 is pressure at 100 mm away from the plate middle.

Fig. 7 compares the plate nodal velocities and deflections from the experiment and from the ALE simulation. The deflection velocity at plate midpoint is in good agreement with the experiment. The rigid-body velocity is well captured in magnitude, but there is a substantial phase difference. It seems that the rigid-body velocity is in phase with the mid-plate deflection velocity, but this is not observed from the experiment. The resulting plate deflection agrees reasonably well with the experimental curve.

The above results show that the ALE simulation reproduces the water-entry experiments of rigid and deformable bodies reasonably well. It is therefore concluded that the present slamming modelling and numerical set-ups are reasonably sound and can be applied for the hydro-plastic slamming analysis of beams and stiffened plates.

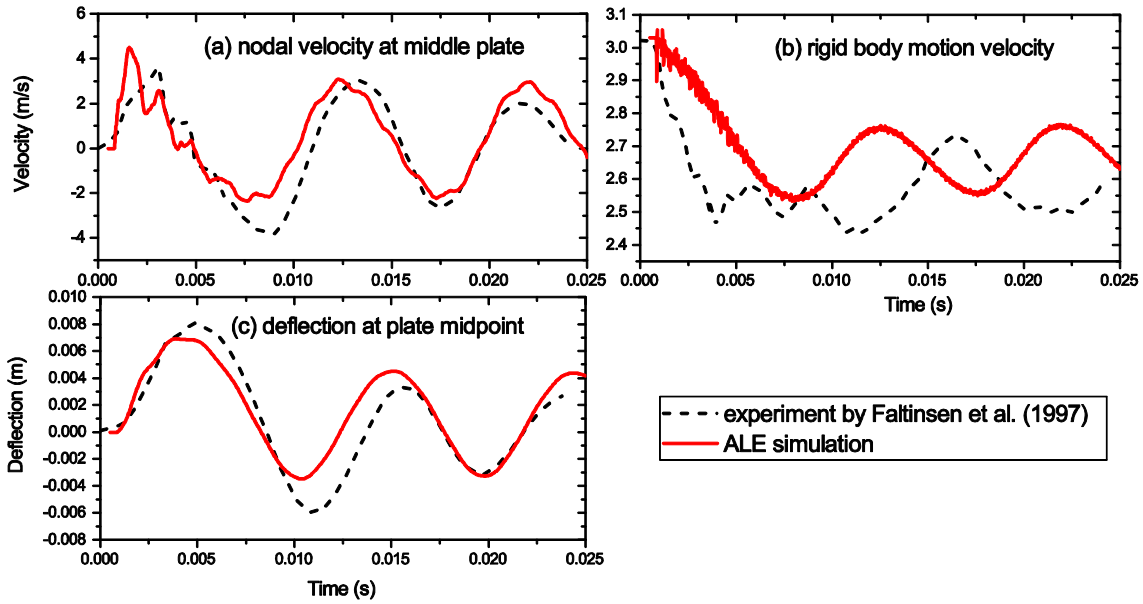


Fig. 7. Comparison of (a) nodal velocity at middle plate, (b) rigid motion velocity and (c) deflection at plate middle point from experiment and ALE simulations

## 4. ALE simulation of hydro-plastic slamming of beams and stiffened panels

Numerical set-ups and convergence tests for the ALE simulation of hydro-plastic slamming are described in this section. The steel material with a yield stress of 355 MPa is used for the plates and stiffened panels. A linear hardening model with a small hardening stiffness is used to reduce the influence of hardening as the analytical model assumes an elastic-perfectly plastic material. The parameters for the material are shown in Table 4.

Table 4. Material properties for the plates and stiffened panels

| *Material* | *Density (kg/m$^3$)* | *Hardening type* | *$\sigma_y$ (MPa)* | *E (GPa)* | *$E_t$ (MPa)* |
|---|---|---|---|---|---|
| steel | 7850 | Linear | 355 | 207 | 400 |

### *4.1 Water entry of flat plates*

For the 2D water entry simulation of flat plates, a water domain with dimensions of 3 m×2 m and an air domain of 3 m×1 m were established (refer Fig. 8). The flat plate is 1m in length. The plate boundary nodes are fixed against all degrees of freedom except for the vertical *z* direction. One shell element is modelled in the thickness direction. The fluid nodes are fixed in *y* direction to enable a 2D condition. A convergence test is carried out to determine the mesh size for the fluid and structure domains in *Section 4.3*. The plate thickness is set as 3 mm, 6 mm, 10 mm or 20 mm with an initial impact velocity of 5 m/s, 10 m/s or 15 m/s.

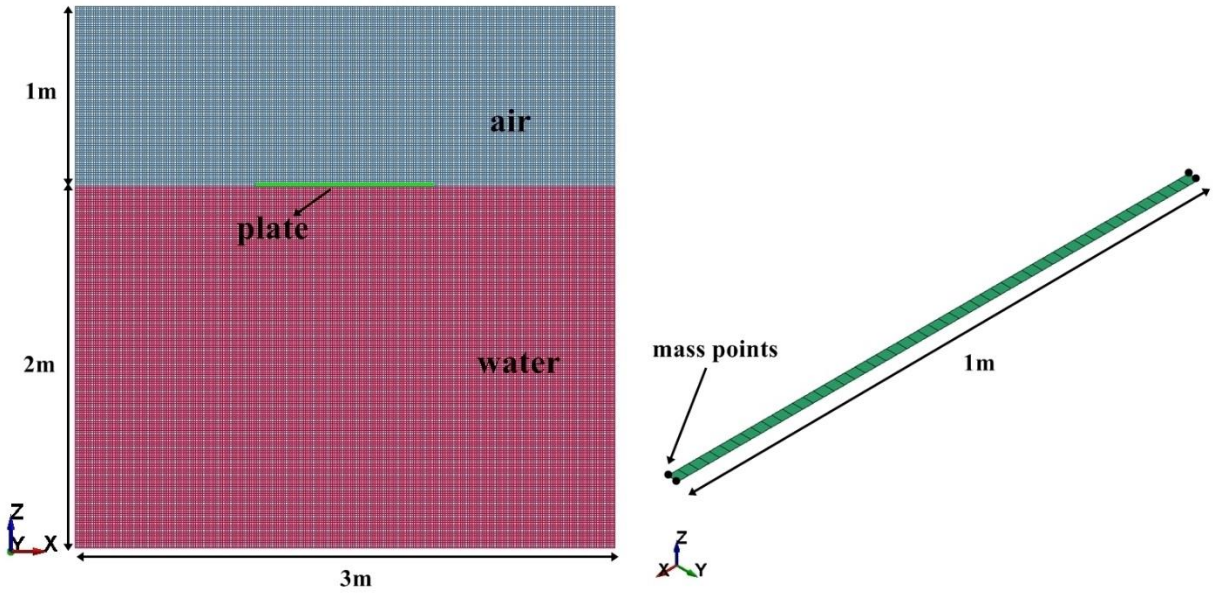


Fig. 8. Left: modelling of water entry of a flat plate; Right: numerical plate

### *4.2 Water entry of stiffened panels*

For 2D water entry simulation of stiffened panels, the water and air domains are modeled with the dimensions of 4 m×2 m and 4 m×1.5 m, respectively, (refer Fig. 9). In the thickness direction, the domain extension equals the spacing between stiffeners. In order to verify the analytical model comprehensively, 6 stiffener cross sections are modelled, covering different area ratios, panel lengths and panel thicknesses.

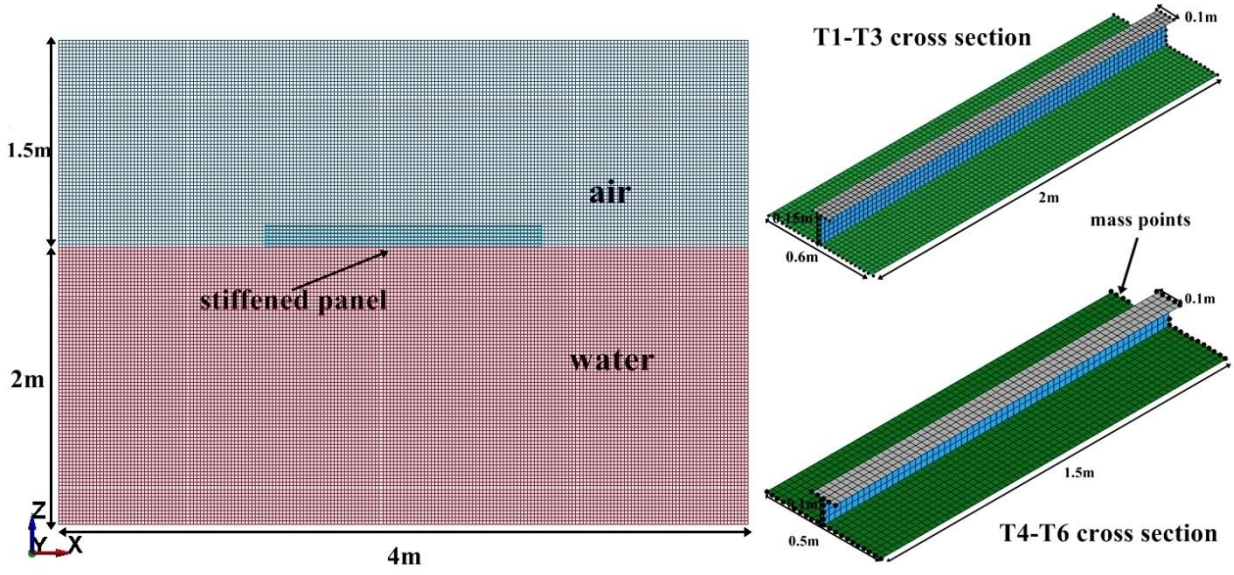


Fig. 9. Left: modelling of water entry of a stiffened panel. Right: different geometries of the numerical panel

The dimensions are given in Table 5. The panel stiffness varies from weak to strong, yielding large to small permanent deflections for a given initial impact velocity. Different cases for water entry of flat stiffened panels are simulated with the initial impact velocity being 7 m/s, 10 m/s or 15 m/s.

The fluid nodes are fixed in *y* direction to enable a 2D flow condition. The plate boundary nodes are fixed against all degrees of freedom except for the vertical *z* direction. The mesh sizes for the fluid domain and structures are determined by a convergence test in *Section 4.3*.

Table 5. Dimensions of different stiffened panel cross sections (Unit: mm)

| *Cross section type* | *Length* | *Plate flange* | *Web* | *Top flange* | $A_p/A_s$ | $A_w/A_t$ |
|---|---|---|---|---|---|---|
| T1 | 2000 | 600 x 5 | 150 x 10 | 100 x 10 | 1.2 | 1.5 |
| T2 | 2000 | 600 x 10 | 150 x 10 | 100 x 10 | 2.4 | 1.5 |
| T3 | 2000 | 600 x 15 | 150 x 15 | 100 x 15 | 2.4 | 1.5 |
| T4 | 1500 | 500 x 8 | 100 x 8 | 100 x 8 | 2.5 | 1 |
| T5 | 1500 | 500 x 10 | 100 x 15 | 100 x 15 | 1.67 | 1 |
| T6 | 1500 | 500 x 15 | 100 x 20 | 100 x 20 | 1.875 | 1 |

### *4.3 Convergence tests with different mesh sizes*

A convergence test is carried out for a flat plate strip with the dimensions 1 m$\times$0.02 m$\times$6 mm impacting the water with an initial velocity of 15 m/s. The fluid and structure mesh sizes are the same. Five different mesh sizes of 100 mm, 50 mm, 25 mm, 10 mm and 5 mm are tested. The resulting plate central deflections are plotted in Fig. 10. The convergence curves of the impulse in the acoustic phase, the total impulse and the maximum plate deflection with decreasing mesh sizes are plotted in Fig. 11.

It is found that the maximum deflections and permanent deflections reduce with decreasing mesh sizes. The trend of the deflection curves becomes similar when the mesh size is equal to or smaller than 50 mm. The magnitude of the deflection curve converges with a mesh size of 10 mm and 5 mm. The impulses in the acoustic phase becomes stable for a mesh size of no larger than 50 mm while the total impulse tends to converge at a mesh size of 10 mm. Considering both efficiency and accuracy, the mesh sizes of the fluid and structure domains are kept the same, and set equal to 10 mm for the water entry of flat plate strips and 25 mm for the water entry of stiffened panels.

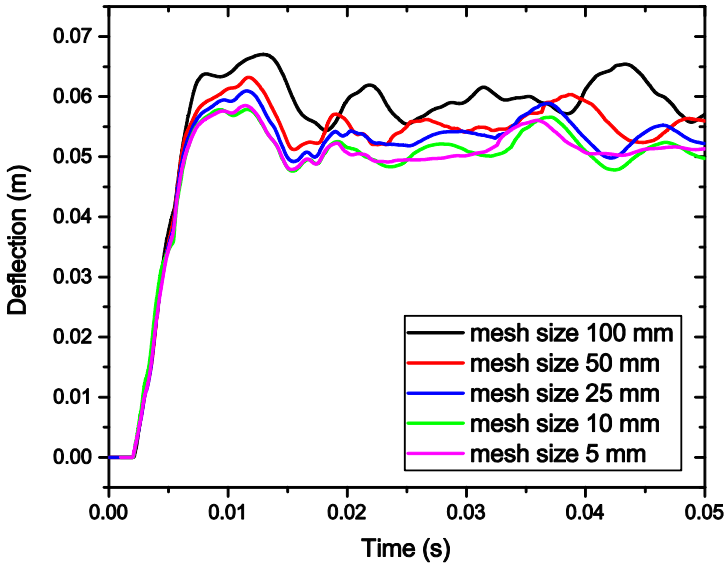


Fig. 10. Plate deflections with different mesh sizes.

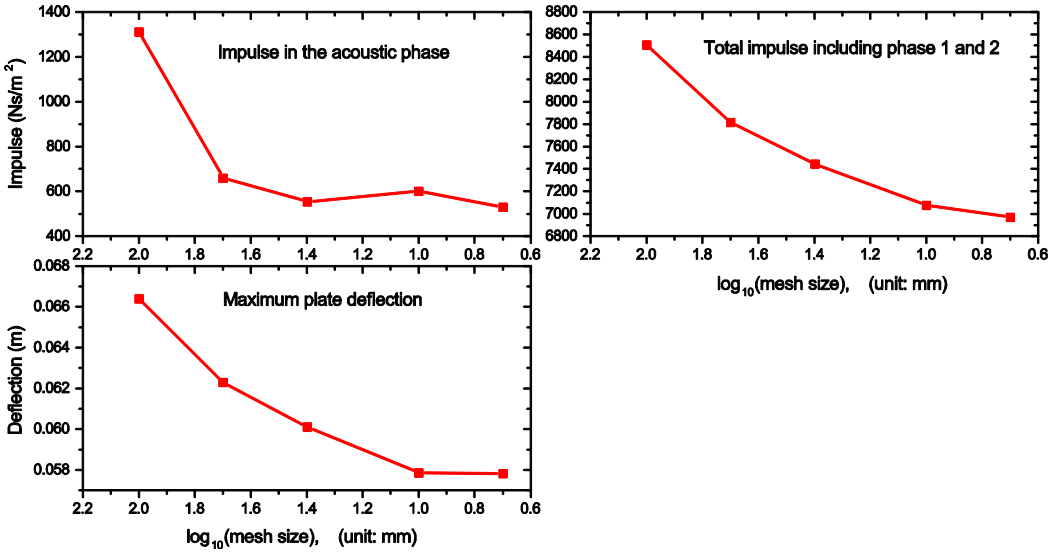


Fig. 11. Plate deflections with different mesh sizes.

### *4.4 Sensitivity of structural responses to different ballast weights*

Plates and stiffened panels subjected to local slamming loads are often part of a large structural system with significant mass, e.g. a ship or an offshore platform, such that the global structure remains virtually unmoved during and after slamming. To account for this, large ballast masses should be attached to the slammed structures such that it keeps the initial speed virtually unchanged during and after slamming. To enable this behavior, mass points are distributed uniformly along the boundaries of the slammed structure

A sensitivity analysis was carried out for plates and stiffened panels by varying their ballast masses. The resulting response is plotted in Figs. 12 and 13. The base case for the 2D flat plate water entry is a plate strip with dimensions of 1 m$\times$0.02 m$\times$6 mm impacting the water with an initial velocity of 10 m/s. The mass of the bare plate strip is 0.942 kg. The base case for water entry of stiffened plates is T2 cross section stiffened panel with an initial impact velocity of 15 m/s. The mass of the bare stiffened plate is 133 kg.

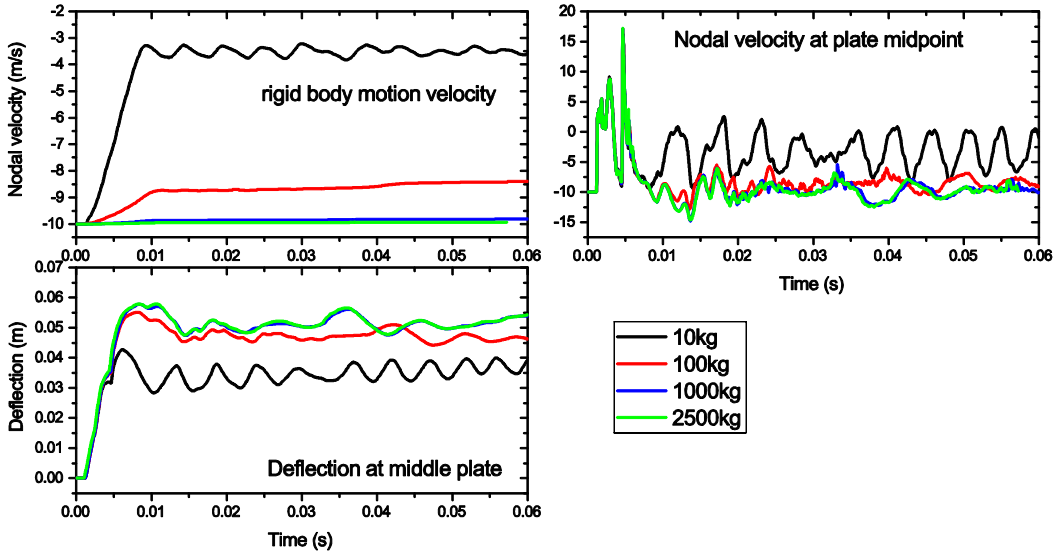


Fig. 12. The response of a flat plate with different total masses during water entry. The dimensions of the plate is 1m×0.02 m× 6 mm, and it impacts the water with an initial velocity of 10 m/s. The mass of the bare plate is around 0.0942 kg.

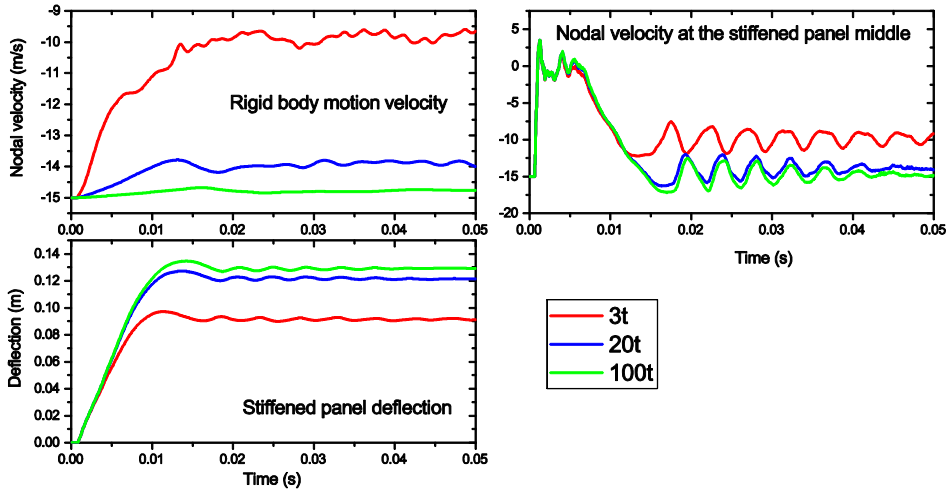


Fig. 13. Response of a stiffened panel with different total masses during water entry. The stiffened panel is with T2 cross section and impacts the water with an initial velocity of 15 m/s. The mass of the bare panel is around 133 kg

Figs. 12 and 13 show that the nodal velocities at the boundaries, representing rigid-body velocities of plate strips and stiffened panels, decrease under slamming loads. The velocity reduction depends on the total mass. For the flat plate strip, a total mass of 10 kg, 100 kg, 1000 kg and 2500 kg yields a velocity reduction of around 65%, 12%, 1.7% and 0.7%, respectively. The rigid motion velocity of a stiffened panel with a total mass of 3 tons, 20 tons and 100 tons decreases by about 33.3%, 6.6% and 2%, respectively.

For water entry of flat plates, the velocity of the plate middle node increases quickly from -10 m/s to a mean value of 0 m/s with some oscillations. Regardless of the total mass, the velocity history at the middle node is very similar before it converges to the rigid body motion velocity at the end of slamming. A similar phenomenon is also found for stiffened panels. The differences in velocities and displacements between the nodes at the boundaries and in the plate middle describe the structural local deformations. The structural deformations tend to converge to a constant value when the total mass is large enough.

In subsequent simulations, a total mass of 2.5 tons and 100 tons is used for water entry simulations of plate strips and stiffened panels, respectively. This yields less than 5 percent reduction of the rigid-body velocities after slamming. For cases with smaller masses, the input velocity for the analytical model should be based on the mean of the rigid-body velocity.

## 5. Comparison of the analytical model and numerical simulations

### *5.1 Water entry of flat plates*

Numerical predictions of the fluid flow and plate deformations are shown in Fig. 14. The plate strips are 1 m in length and 0.02 m in width. The plate thickness is 6 mm and the initial impact velocity is 10 m/s. The corresponding displacement profiles for half a plate with a time interval of 0.4 ms are shown in Fig. 15. They demonstrate that the plate gets a significant change of curvature over a relatively short distance and this may be interpreted as a plastic hinge. As time increases, the instantaneous hinge position, marked as a red point in Fig. 15 at each time instant, moves towards the plate center. It is interesting to notice that the positions of the travelling hinge at different time instants lie virtually on a straight, horizontal line for a time period. This implies that, the deformation velocity at this stage on average counteracts the drop velocity. This is clear evidence that the initial deformation velocity is on average equal to the drop velocity. In addition, the wider view confirms negligible plate deformations within less than 1 ms from the initial impact.

To the left of the travelling hinge, the imposed plastic curvature seems to be fairly constant and the ‘arm’ behind the hinge rotates only as a rigid body. The parallel arms represent major characteristics of the travelling hinge stage. It is found that the rotating arms become no longer parallel to each other before the hinge reaches the beam middle. This is because, the deformation of the thin plate follows *Path 2*, where the pure tension stage 3 is reached but the moving hinges have not met in the middle. From Fig. 15, it seems that it takes more time to reach the pure tension stage in numerical simulations than predicted using the proposed theory. This is due to the large elastic deflections before entering the plastic regime, which is not accounted for in the theory. The plot confirms that the travelling hinge concept is useful in describing the actual displacement field.

With the imposed velocity from the acoustic phase, the plate builds up deformations over time in the free-deflection stage until all the energy is dissipated and the permanent deflection is reached. During this process, water is accelerated upwards, forming jets that leave from the structure sides. A small portion of elastic energy may be released through plate vibrations about the permanent deformations.

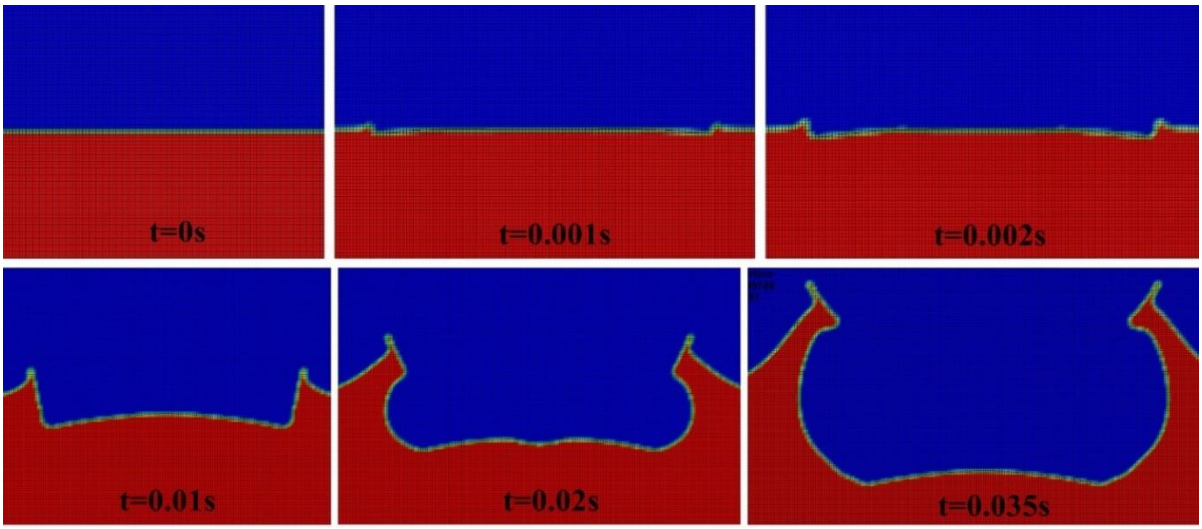


Fig. 14. Snapshots of the plate deformation and flow field during water entry; the plate thickness is 6 mm and the initial impact velocity is 10 m/s

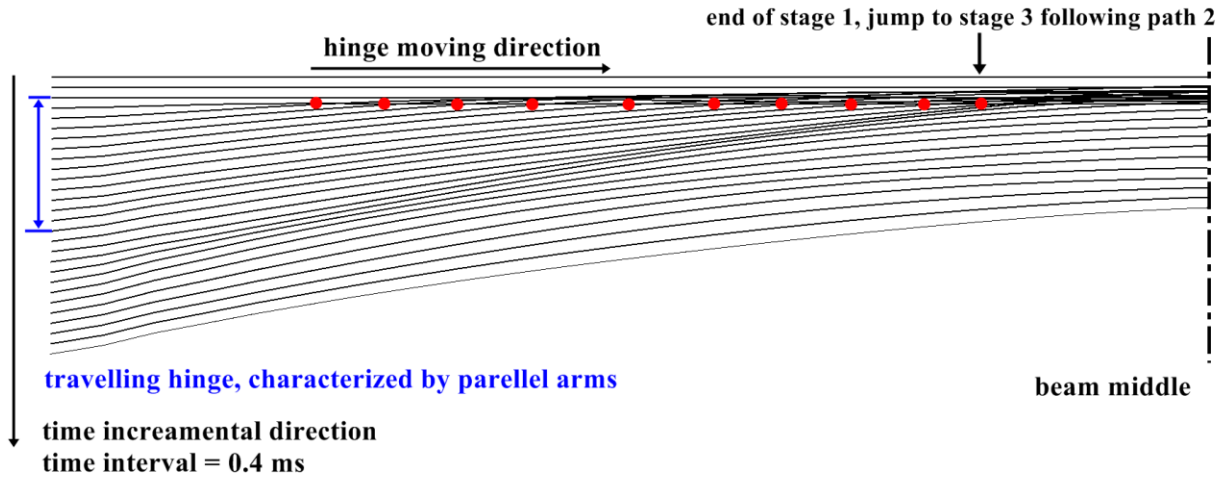


Fig. 15. Snapshots of displacement profiles for half of a plate strip during water entry; the plate thickness is 6 mm and the initial impact velocity is 10 m/s. The time interval is 0.4 ms. The red points denote positions of the travelling hinge at each time instant.

Figs. 16 and 17 plot the average pressure histories for the flat plate with impact velocities of 5 m/s, 10 m/s and 15 m/s and with plate thicknesses of 3 mm, 6 mm, 10 mm and 20 mm. From Fig. 16, the peak pressure increases linearly with increasing impact velocity for given plate dimensions. The peak pressure, however, cannot exceed the acoustic pressure. Proportionality is also found for the impulse of the acoustic stage and the total impulse including the acoustic stage and the free

deflection stage with respect to the impact velocities. This is consistent with the assumption, used in the analytical method, that in the acoustic stage, the structure is imparted an velocity equal to the initial impact velocity $V_0$ in the middle between travelling hinges and linearly decreasing to zero from the travelling hinge to the beam end. If we crudely assume the whole beam velocity is $V_0$, then the impulse in the acoustic stage would be $\rho_m h V_0$ $\left(\text{unit:Ns/m}^2\right)$. Here, $\rho_m$ is the density of the structural material. Figs. 16 and 17 show that $\rho_m h V_0$ is 15%-25% smaller than the impulse in the acoustic stage $I_{acoustic}$.

Fig. 17 shows that the plate stiffness is a crucial factor to determine the peak pressure in the acoustic stage and the slamming duration. Given the same impact velocity of 10 m/s, the peak pressure and impulse of the acoustic stage increase with increasing plate thickness while the slamming duration reduces. It is interesting to find that the total impulse remains virtually the same regardless of the plate thickness.

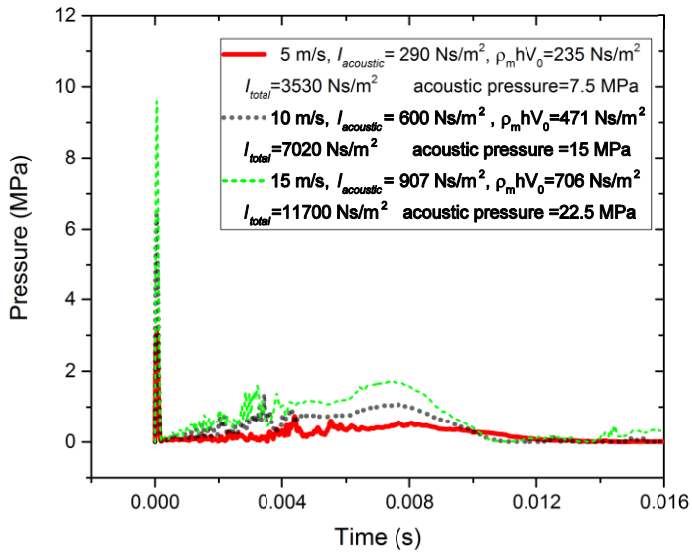


Fig. 16. Average pressure time history over plates with different initial impact velocities; each plate strip has the dimensions of 1 m×0.02 m×6 mm

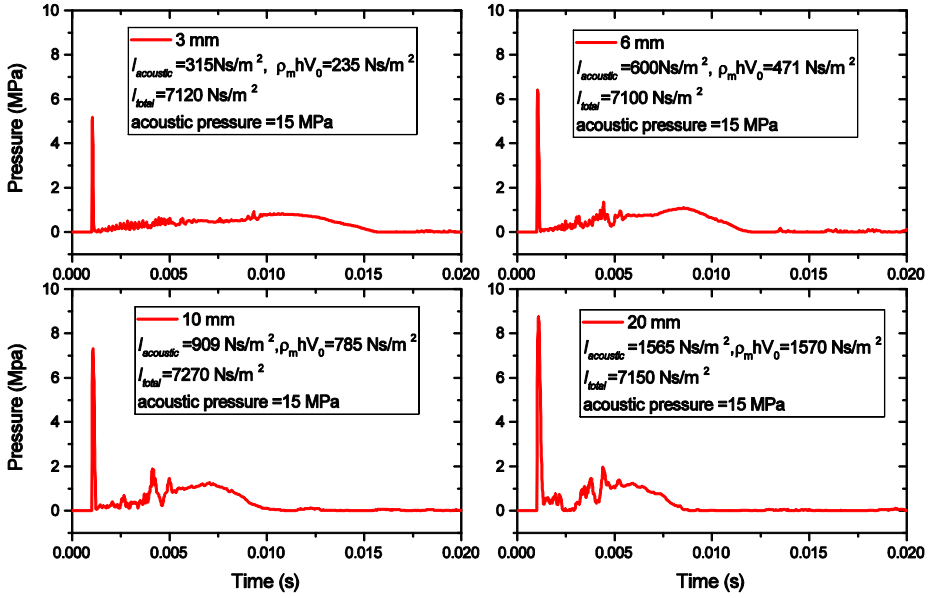


Fig. 17. Average pressure history versus plate thickness with an initial impact velocity of 10 m/s

Fig. 18 compares the central deflections of flat plates with a thickness of 3 mm, 6 mm, 10 mm and 20 mm during 2D water-entry as predicted by ALE simulations and by the proposed analytical model. The initial impact velocity is 10 m/s. The simulations show that the plates deform to their permanent deflections with small elastic oscillations about the mean deformations, and the plastic energy is dominant. Fig. 19 shows the deflection history of the 6 mm plate with an initial impact velocity of 5 m/s, 10 m/s and 15 m/s. From Figs. 18 and 19, the permanent deflections predicted with the analytical model agree well with those from the ALE simulations for the selected plate thickness and impact velocity ranges. It is observed that the permanent deflection is somewhat overestimated especially for small impact velocities. This is mainly because the analytical model assumes that all energy is dissipated by the plastic deformation and the elastic energy is neglected. It is interesting to find from Figs. 16 and 19 that the durations of the acoustic and the free-deflection stage remain virtually insensitive to the initial impact velocity. Permanent deflections are reached virtually at the same time for all velocities.

The non-dimensional permanent deflections of plate strips are plotted versus the non-dimensional velocity in Fig. 20 for different mass ratios. Reasonable agreement with ALE simulations is demonstrated. The numerical results confirm that the non-dimensional velocity is dominant. One of the ALE data point deviates slightly from the curve because the elastic energy becomes important in this case.

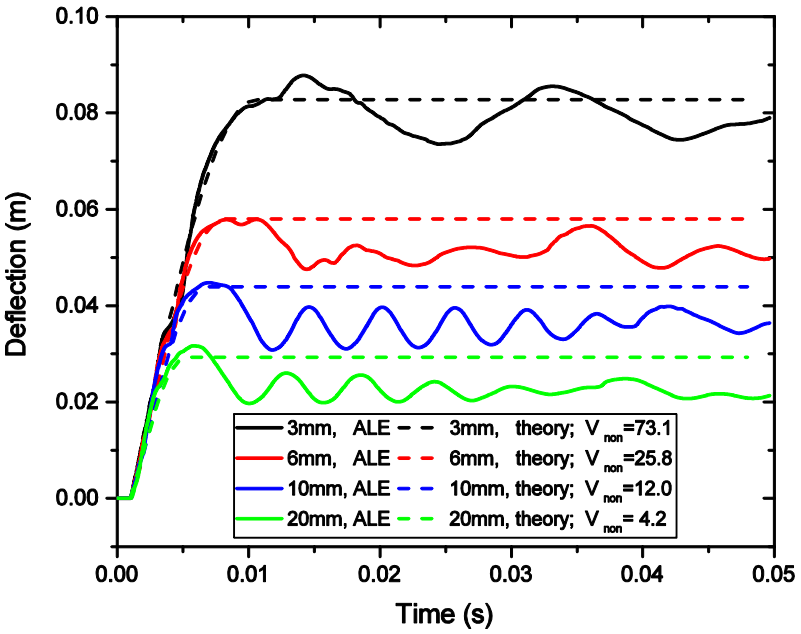


Fig. 18. Plate deflections for different thicknessnes during water entry with an initial velocity of 10 m/s

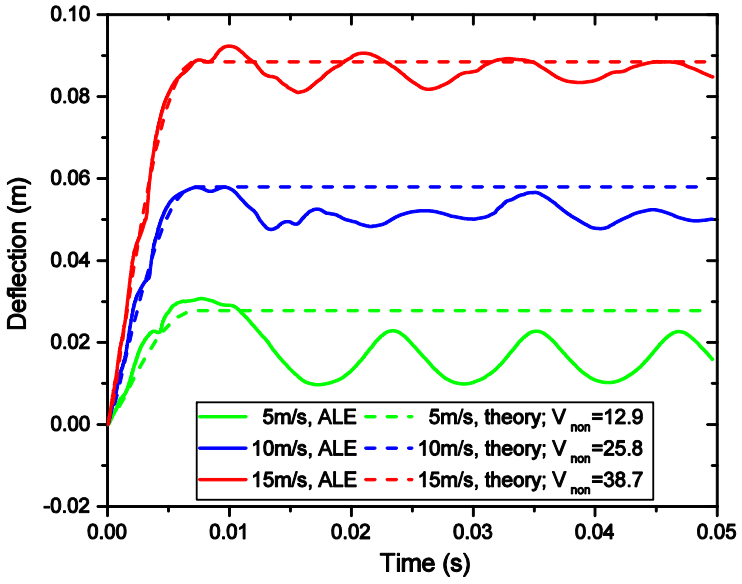


Fig. 19. Plate deflections for different initial velocities during water entry; plate thickness t = 6 mm

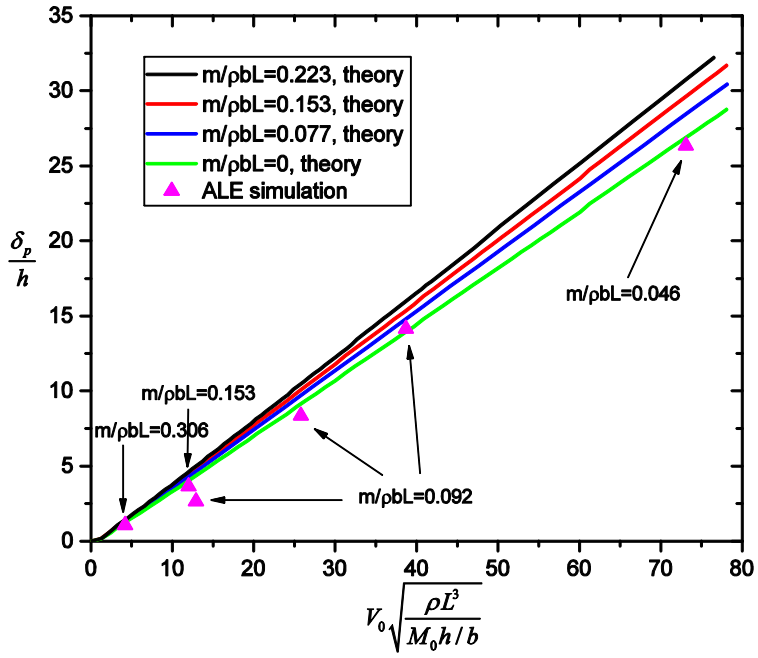


Fig. 20. Non-dimensional permanent deflection versus non-dimensional velocity curves from the analytical model and the corresponding data from ALE simulations during slamming

### *5.2 Water entry of flat stiffened panels*

The general features of the fluid flow during water entry of stiffened panels are quite similar to those shown in Fig. 14 for flat plates. The T3 stiffened panel deformations with an initial impact velocity of 10 m/s are shown in Fig. 21. The panel is subjected to significant plastic flow at the supports and the beam middle span, and undergoes large plastic deformations.

Time histories of the average pressure for panels with T1-T3 cross sections with an initial drop velocity of 10 m/s are plotted in Figs. 22 (a) and (b). The pressure histories for panel T2 are plotted as a function of the drop velocity in Figs. 22 (c) and (d). According to the velocity assumption, the momentum change due to the structural deformation is approximately $\rho_m V_0 A_e / b$ $\left(\text{unit:Ns/m}^2\right)$. The $\rho_m V_0 A_e / b$ values for stiffened panels are very close to the impulse predicted in the acoustic phase by the ALE simulations (refer Figs. 22 (a) and (c)). This justifies the assumption of an initial uniform deformation velocity equal to $V_0$ in the free deflection phase. Based on the similarity of the pressure impulse for rigid and deformable panels in the acoustic phase, it may become reasonable to measure the pressure impulse in the acoustic phase on rigid plates, and use the impulse to calculate the deformation velocity of the deformable structure. From Figs. 22 (c) and (d), the pressure histories are generally in phase while the magnitude increases with velocity. The impulses in the acoustic phase and the total impulses increase with the velocity as well.

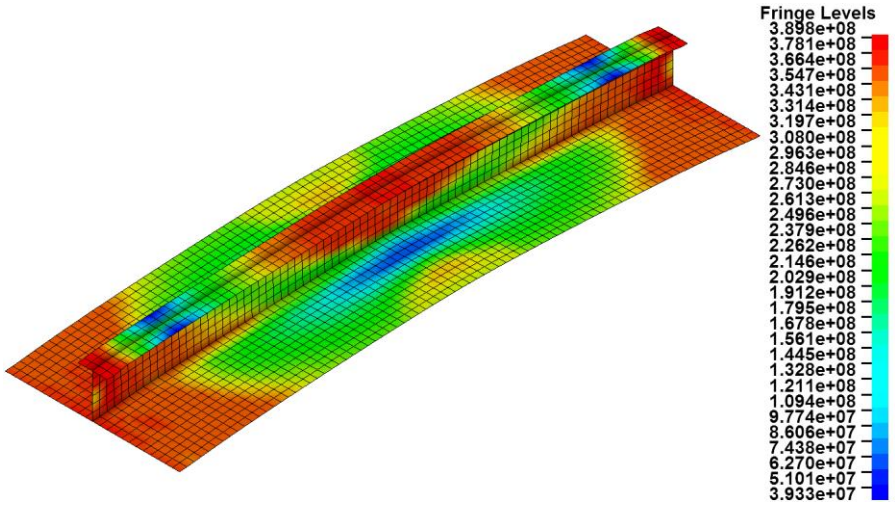


Fig. 21. Deformation and the von-Mises equivalent stresses (unit, Pa) of the T3 stiffened panel under slamming loads as predicted by the ALE simulation. The initial impact velocity is 10 m/s.

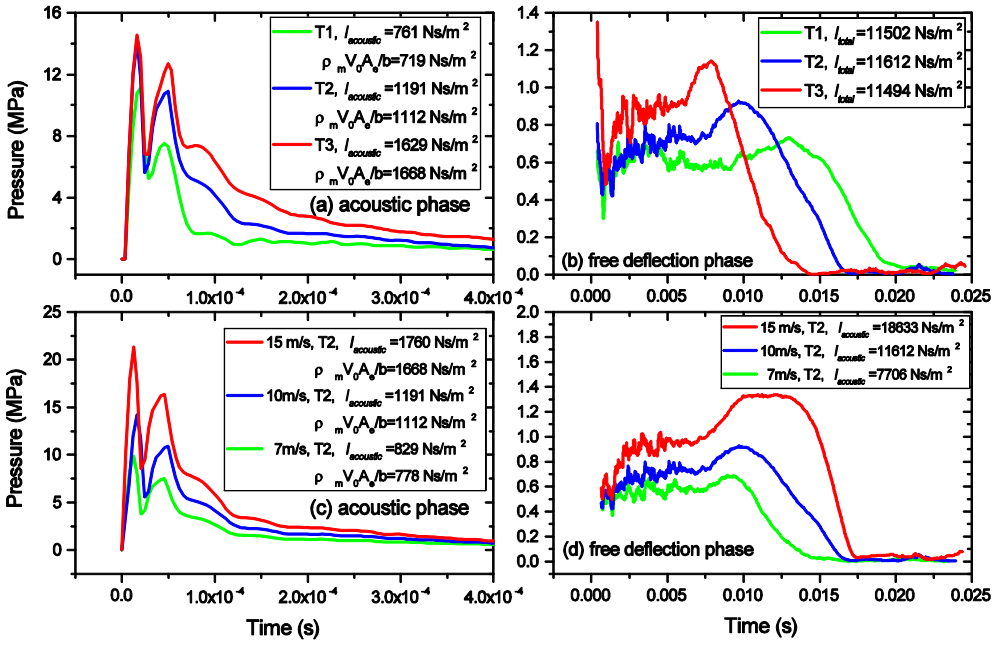


Fig. 22. Average pressure histories predicted by the ALE simulations for (a) stiffened panels T1-T3 with an initial drop velocity of 10 m/s in the acoustic phase, (b) stiffened panels T1-T3 with an initial drop velocity of 10 m/s in the free deflection phase, (c) stiffened panel T2 with different initial velocities in the acoustic phase, (d) stiffened panel T2 with different initial velocities in the free deflection phase

Figs. 23 and 24 compare central deflections of flat stiffened panels with 6 different cross sections during 2D water entry predicted by LS-DYNA ALE simulations and by the analytical model. The stiffened panels cover different beam lengths, $A_p/(A_w+A_t)$ ratios and $A_w/A_t$ ratios. The initial impact velocity is 10 m/s for T1-T3 stiffened panels and 15 m/s for T4-T6 stiffened panels. Figs.

25 and 26 compare the deflections for the T2 and T5 stiffened panels, respectively, with the initial impact velocity being 7 m/s, 10 m/s and 15 m/s.

The results show that the analytical model predicts the deflection curves of stiffened panels quite reasonably both in phase and in magnitude. It overestimates slightly the deflection for small impact speeds. One main reason is the rigid perfectly plastic material assumption adopted for the steel without considering the elastic effect. Another reason is that the initial position of the travelling hinge is determined by assuming that the peak pressure is equal to the acoustic pressure, but in reality the true pressure should be smaller (see e.g. Fig. 22). This underestimates the distance of the initial travelling hinge position to the supports, i.e. $X\left(t=0\right)$, and thus overestimates the permanent deflections. Considering the complexity of the problem, the proposed analytical model provides fairly good accuracy.

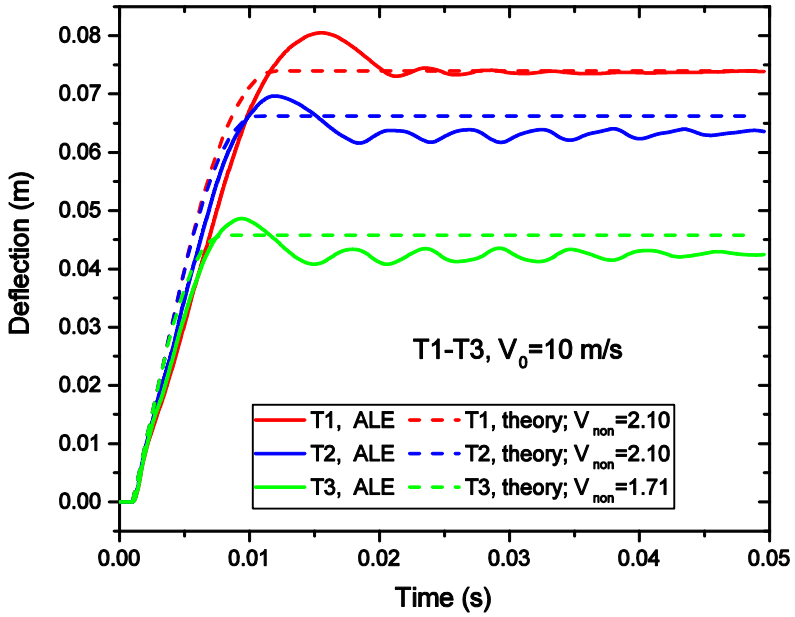


Fig. 23. Deflections of stiffened panels with cross sections of T1, T2 and T3 during water entry. The initial impact velocity is 10 m/s

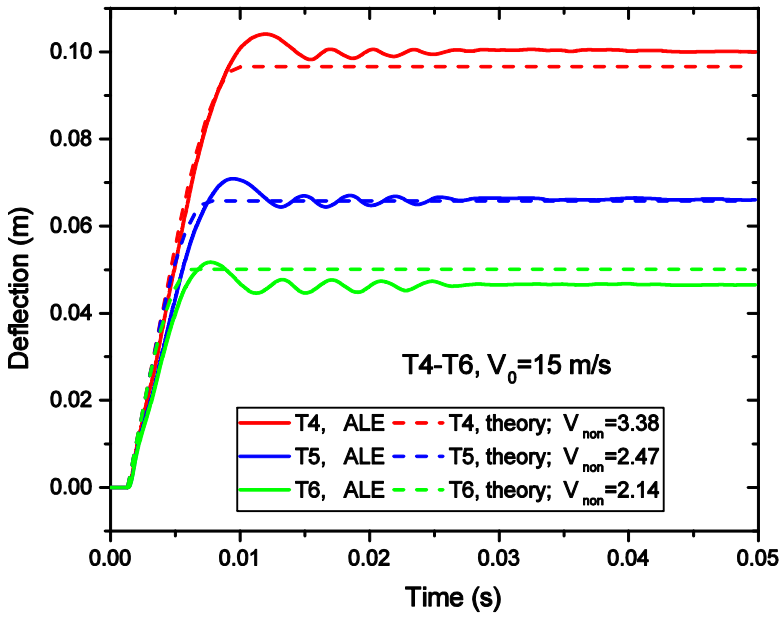


Fig. 24. Deflections of stiffened panels with cross sections of T4, T5 and T6 during water entry. The initial impact velocity is 15 m/s

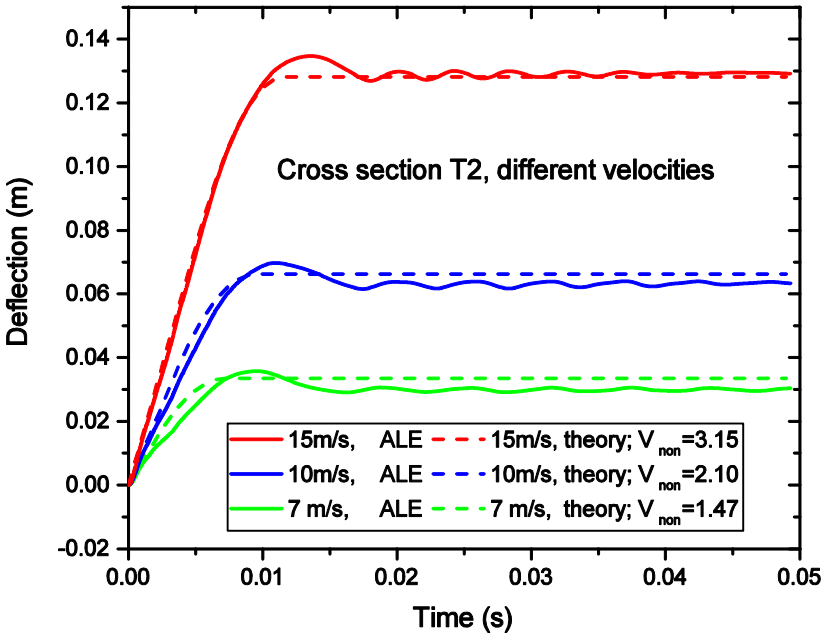


Fig. 25. Deflections of T2 stiffened panels with different initial impact velocities during water entry

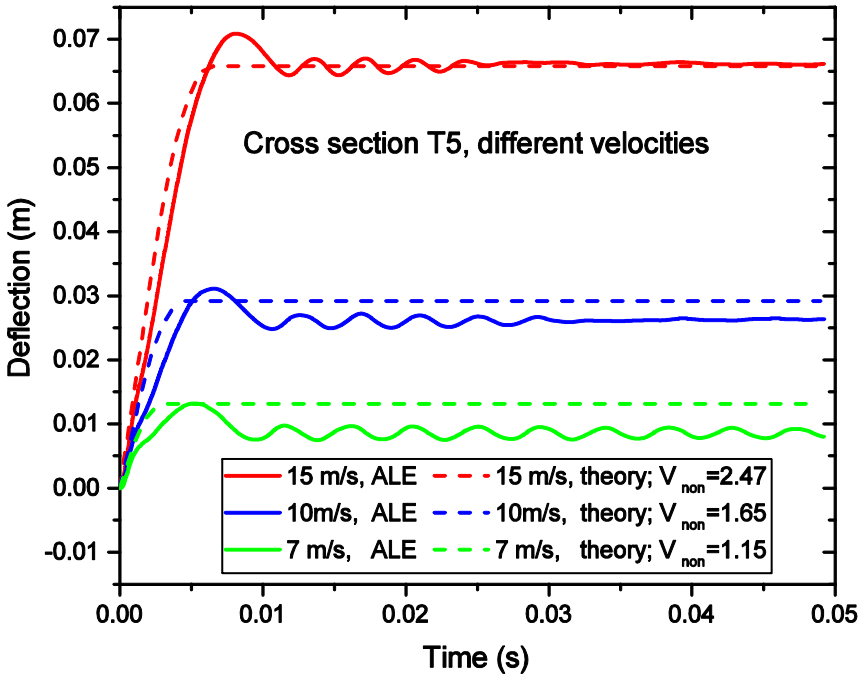


Fig. 26. Deflections of T5 stiffened panels with different initial impact velocities during water entry

Fig. 27 plots the non-dimensional permanent deflections versus the non-dimensional velocity for different $A_p$ / $A_s$ and $A_w$ / $A_t$ ratios for stiffened panels. The non-dimensional velocity is dominant, but the $A_p$ / $A_s$ and $A_w$ / $A_t$ ratios are also important. The design curves are compared with data points from ALE simulations. Results show that the non-dimensional curves compare reasonably with ALE simulations.

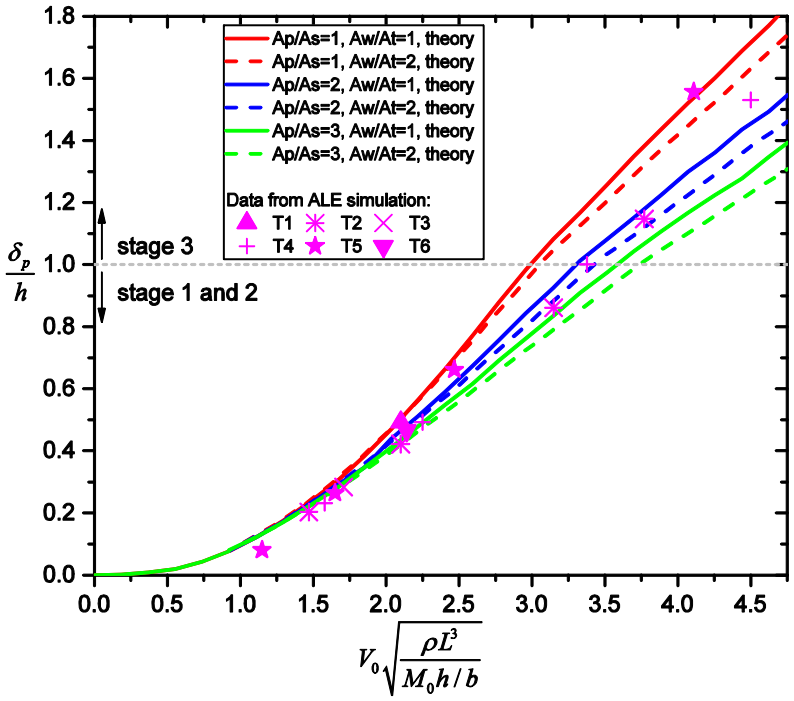


Fig. 27. Non-dimensional permanent deflection of stiffened panels versus non-dimensional velocity curves from the analytical model, and the data from ALE simulations during slamming

### *5.3 Discussion*

The proposed analytical model has shown good accuracy in predicting the permanent deflections of flat plates and stiffened panels during water impact when the elastic energy is small relative to the total energy. However, when the elastic energy is comparable to the total energy, the accuracy decreases. It is interesting to assess quantitatively how much the elastic energy may occupy for different cases.

For uniform pressure loaded beams, the bending moment diagram is shown in Fig. 28. It is assumed that the maximum elastic energy of the beam is obtained when the bending moments at the supports and at the beam middle are equal to $M_0$. $M_0$ is the fully plastic bending moment of the cross section. Then, the bending moment distribution along the beam $M(x)$ is:

$$M(x) = M_0\left(1 - \frac{4x}{L} + \frac{2x^2}{L^2}\right) \tag{1}$$

Thus, the maximum elastic energy in the beam is:

$$E_{elastic,\max} = \frac{1}{2}\int_0^{2L} \frac{M(x)^2}{EI}dx = \frac{7M_0{}^2L}{15EI} \tag{2}$$

where $I$ is the second order moment of inertia of the cross section.

It is assumed that the total kinetic energy can be approximated by $0.5(m_s + m_a)V_0^2$, where $m_s$ is the structural mass and $m_a$ is approximated by the added mass in stage 2, i.e. $m_a = \pi / 4 \cdot \rho b L^2$.

Thus, the ratio of the maximum elastic energy relative to the total kinetic energy is:

$$\frac{E_{elastic,\max}}{E_{kinetic,tot}} = \frac{7M_0^{\ 2}}{15EIV_0^2\left(\rho_m A_e + \frac{\pi}{8}\rho bL\right)} \tag{3}$$

where $A_e$ is the area of the cross section, $E$ is the elastic modulus of the material and $\rho_m$ is the density of the structure material. Eq. (3) shows that the maximum elastic energy ratio can be significantly influenced by the impact velocity.

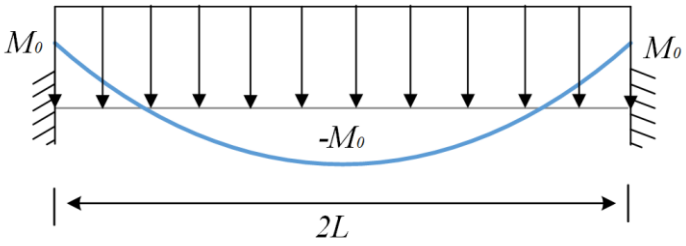


Fig. 28. Bending moment diagram for pressure loaded beams with fixed ends

Table 6 shows ratios of the maximum elastic energy over the total kinetic energy for the simulated cases according to eq. (3). The ratio of the maximum elastic energy is typically smaller than 10 percent. For the case of flat plate impact with a thickness of 6 mm and an initial impact velocity of 5 m/s, the maximum elastic energy is 20.7 percent of the total energy, which is substantial. In this case, the permanent deflection predicted by the analytical model is much larger than the value obtained from the ALE simulation. Based on this verification study, the analytical model can be used with reasonable accuracy for cases with $E_{elastic,max} / E_{kinetic,tot}$ ratios smaller than 10-15 percent.

Table 6. The ratios of elastic energy relative to the total kinetic energy for different cases

| scenario | thickness (mm) /cross section | velocity (m/s) | $E_{elastic,max}/E_{kinetic,tot}$ |
|---|---|---|---|
| plate | 3 | 10 | 2.9% |
| plate | 6 | 10 | 5.2% |
| plate | 10 | 10 | 7.7% |
| plate | 20 | 10 | 11.9% |
| plate | 6 | 5 | 20.7% |
| plate | 6 | 15 | 2.3% |
| stiffened panel | T1 | 10 | 3.7% |
| stiffened panel | T2 | 10 | 2.9% |
| stiffened panel | T3 | 10 | 4.4% |
| stiffened panel | T4 | 10 | 3.1% |
| stiffened panel | T5 | 10 | 6.7% |
| stiffened panel | T6 | 10 | 8.9% |

| | | | |
|---|---|---|---|
| stiffened panel | T5 | 7 | 13.7% |
| stiffened panel | T5 | 15 | 3.0% |
| stiffened panel | T2 | 7 | 5.9% |
| stiffened panel | T2 | 15 | 1.3% |

The analytical model assumes that the locally slammed structures are part of a global structure with a significant mass such that the rigid-body velocity of the local structure remains virtually unchanged during water entry, but in practice the total mass may not be large enough to keep the rigid-body velocity constant. For such cases, the mean rigid-body velocity before and after water entry should be used as input for the model. Fig. 29 compares the deflections of plates and stiffened panels with finite ballast weights. ALE simulation results for both cases have been presented in Figs. 12 and 13 respectively in conjunction with the sensitivity study of ballast weights. The considered flat plate strip is 1 m×0.2 m× 6 mm in dimensions, and it impacts water with an initial velocity of 10 m/s. The total mass including the ballast weight is 10 kg. During water entry, the rigid body motion velocity drops from 10 m/s to 3.5 m/s (refer Fig. 12), and therefore a mean velocity of 6.75 m/s is used as input in the analytical model. The considered stiffened plate is with T2 cross section and impacts the water with an initial velocity of 15 m/s. The total mass including the ballast weight is 3 tons. During the water entry, the rigid-body motion velocity drops from 15 m/s to about 10 m/s (refer Fig. 13), and therefore a mean velocity of 12.5 m/s is used as input.

The results show that the permanent deflections are well predicted with the mean rigid-body motion velocity. However, the deflection curves are no longer in phase with the ALE simulation curves. The difference is due to the gradually changing rigid-body velocity, but permanent deflections are still well captured.

To be consistent with the analytical model, the ALE simulations assumed a material with little hardening. In practice, the strain hardening can be significant for marine steels. In addition, the slamming phenomenon is highly impulsive, and the strain rate effect can be important, but has not been considered here. Both the strain hardening and the strain rate effect increase the material strength, yielding a lower permanent deflection. The proposed model is thus conservative in this respect. Local buckling may occur for panels with slender stiffener webs, and cross-sections with large $A_w/A_t$ ratios are more susceptible to torsional buckling. Both effects are not included in the developed model. However, Yu et al. (2018) found that as long as local tripping or buckling do not occur in the early stages of the deformation, the model is reasonably accurate for stiffened panels. This is because membrane forces mainly govern the resistance at late stages of deformation, and local buckling will then have limited effect. In addition, the effect of local buckling and the neglect of strain hardening counteract to some extent. More validation work on different stiffened panel dimensions should be carried out.

The analytical model assumes that beams can go through unlimited deformations, but in reality, the beam deflection will be limited by material fracture. As a final remark, the analytical formulation calculates the plastic response of beams and stiffened panels through the interaction of the axial force and bending moment neglecting the shear effect. Therefore, it is not recommended to apply the model for beams with $2L/h \leq 8$, where shear forces become significant.

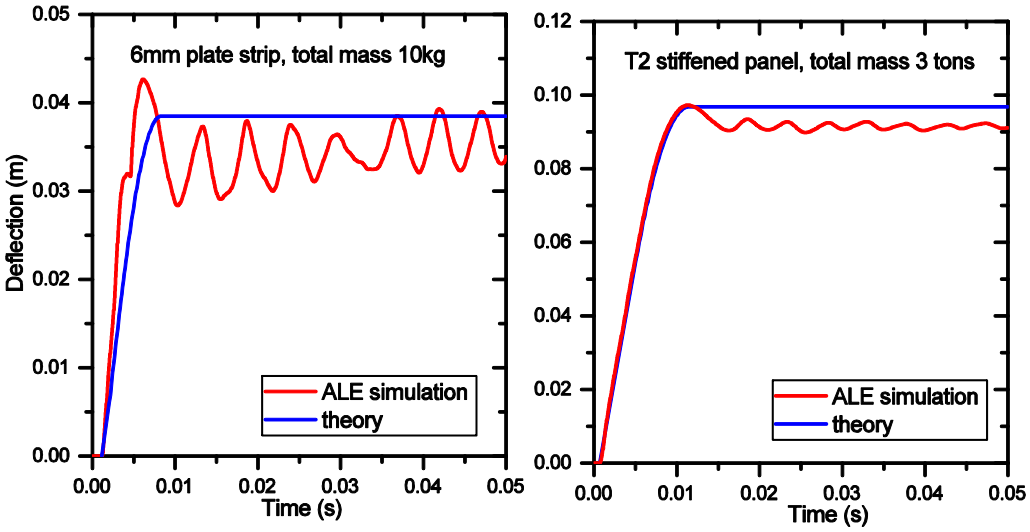


Fig. 29. Deflection of plates and stiffened panels with finite ballast weights

## 6. Conclusions

This Part II of the two-part companion paper verifies the analytical model proposed in Part I by comparing model predictions with results from the multi-material ALE simulations. The modelling and numerical settings of the ALE simulations were validated by comparison with water-entry experiments of a *rigid* wedge and a flat *elastic* plate. Hydro-elastoplastic simulations were carried out for beams and stiffened panels, and the results were discussed. The following conclusions are drawn:

1. The proposed hydro-plastic model is capable of predicting large inelastic permanent deflections of plates and stiffened panels during flat or nearly flat water impacts with good accuracy both in magnitude and in phase. The coupling between hydrodynamic loads and structural deformations is well captured. The model works well when the ratio of the elastic energy relative to the total kinetic energy is less than 15%.

2. A key element of the theoretical model is the travelling hinge concept used to describe the structural deformation. The validity of the concept is confirmed from the snapshots of displacement profiles of plate strips from the hydro-elastoplastic slamming ALE simulations.

3. In the acoustic stage, the maximum pressure increases with the impact velocity and the structural stiffness, and the impulse imparted to the structures is close to the structural momentum with a deformation velocity equal to the initial impact velocity. In the free deflection phase, the interaction with hydrodynamic actions is important. The pressure in this phase is lower but the duration is significantly longer. The total impulse including the acoustic phase and the free-deflection phase is proportional to the impact velocity regardless of the structural stiffness. The rising time, however, is determined by structural stiffness and not sensitive to the initial impact velocity.

4. The non-dimensional diagrams for the permanent deflection of plate strips and stiffened panels as a function of the impact velocity, have been proved useful by comparison with ALE simulations.

The simplicity of the diagrams makes them good candidates to be utilized in rules and standards concerned with design against extreme water slamming in ULS and ALS conditions.

## Acknowledgments

This work has been funded by the Research Council of Norway (NFR) through the Centers of Excellence funding scheme, project AMOS (Grant number 223254) at the Norwegian University of Science and Technology (NTNU). This support is gratefully acknowledged by the authors.

## References

BAE, D.-M. & ZAKKI, A. F. 2011. Comparisons of Multi Material ALE and Single Material ALE in LS-DYNA for Estimation of Acceleration Response of Free-fall Lifeboat. *Journal of the Society of Naval Architects of Korea,* 48**,** 552-559.

BISHOP, R. E. & PRICE, W. G. 1979. *Hydroelasticity of ships*, Cambridge University Press.

CHEON, J. S., JANG, B.-S., YIM, K. H., LEE, H. D., KOO, B.-Y. & JU, H. 2016. A study on slamming pressure on a flat stiffened plate considering fluid–structure interaction. *Journal of Marine Science and Technology,* 21**,** 309-324.

DNVGL-OTG-13 2016. Prediction of air gap for column stabilised units. *offshore technical guidance*.

DNVGL-OTG-14 2016. Horizontal wave impact loads for column stabilised units. *Offshore Technical Guidance*.

FALTINSEN, O. M. 2000. Hydroelastic slamming. *Journal of Marine Science and Technology,* 5**,** 49-65.

FALTINSEN, O. M., KVÅLSVOLD, J. & AARSNES, J. V. 1997. Wave impact on a horizontal elastic plate. *Journal of Marine Science and Technology,* 2**,** 87-100.

HALLQUIST, J. O. 2007. LS-DYNA keyword user's manual. *Livermore Software Technology Corporation,* 970**,** 1-2.

HENKE, D. J. 1994. Transient response of plates to travelling loads with application to slamming damage. *International journal of impact engineering,* 15**,** 769-784.

JIANG, J. & OLSON, M. 1995. Rigid-plastic analysis of underwater blast loaded stiffened plates. *International journal of mechanical sciences,* 37**,** 843-859.

JONES, N. 2011. *Structural impact (second edition)*, Cambridge university press.

KVALSVOLD, J. & FALTINSEN, O. M. 1995. Hydroelastic modelling of wet deck slamming on multihull vessels.

LUO, H., HU, J. & GUEDES SOARES, C. 2010. Numerical Simulation of Hydroelastic Responses of Flat Stiffened Panels Under Slamming Loads. 373-381.

QIN, Z. & BATRA, R. C. 2009. Local slamming impact of sandwich composite hulls. *International Journal of Solids and Structures,* 46**,** 2011-2035.

SHIN, H., SEO, B. & CHO, S.-R. 2017. Experimental investigation of slamming impact acted on flat bottom bodies and cumulative damage. *International Journal of Naval Architecture and Ocean Engineering*.

SKJEGGEDAL, E. 2017. *Wave-in-Deck Forces and Response of Semi-Submersibles.* NTNU.

STENIUS, I., ROSÉN, A. & KUTTENKEULER, J. 2006. Explicit FE-modelling of fluid–structure interaction in hull–water impacts. *International Shipbuilding Progress,* 53**,** 103-121.

WANG, S., KARMAKAR, D. & SOARES, C. G. 2016. Hydroelastic impact of a horizontal floating plate with forward speed. *Journal of Fluids and Structures,* 60**,** 97-113.

YAMADA, Y., TAKAMI, T. & OKA, M. Numerical study on the slamming impact of wedge shaped obstacles considering fluid-structure interaction (FSI). The Twenty-second International Offshore and Polar Engineering Conference, 2012. International Society of Offshore and Polar Engineers.

YU, Z. & AMDAHL, J. 2018. A review of structural responses and design of offshore tubular structures subjected to ship impacts. *Ocean Engineering,* 154**,** 177-203.

YU, Z., AMDAHL, J., GRECO, M. & XU, H. 2019. Hydro-plastic response of beams and stiffened panels subjected to extreme water slamming at small impact angles, Part I: An analytical solution. *Marine Structures*.

YU, Z., AMDAHL, J. & SHA, Y. 2018. Large inelastic deformation resistance of stiffened panels subjected to lateral loading. *Marine Structures,* 59**,** 342-367.

ZHAO, R., FALTINSEN, O. & AARSNES, J. Water entry of arbitrary two-dimensional sections with and without flow separation. Proceedings of the 21st symposium on naval hydrodynamics, 1996. Trondheim, Norway, National Academy Press, Washington, DC, USA, 408-423.